


Cite this: *RSC Adv.*, 2021, 11, 18605

Received 31st March 2021  
Accepted 9th May 2021

DOI: 10.1039/d1ra02525b

rsc.li/rsc-advances

# $\text{TM}_4\text{B}_{18}^{0/-}$ (TM = Hf, Ta, W, Re, Os): new structure construction with TM doped B wheel units†

Zhen Wang, Qiuying Du and Sung Jin Park \*

We report the global search for the lowest energy structures of the transition metal (TM) doped B clusters,  $\text{TM}_4\text{B}_{18}^{0/-}$  (TM = Hf, Ta, W, Re, Os) and their electronic properties. A combination of the comprehensive genetic algorithm (CGA) method with density functional theory (DFT) calculations shows that they are composed of four planar  $\text{TM@B}_9$  wheel units by sharing B atoms, except for  $\text{Os}_4\text{B}_{18}^{0/-}$ , which consists of two types of planar molecular wheels of  $\text{Os@B}_7$  and  $\text{Os@B}_8$ . Among these nanoclusters, it is found that the  $\text{Ta}_4\text{B}_{18}$  cluster has a closed-shell with a large HOMO–LUMO gap of 2.61 eV. Adaptive natural density partitioning analysis (AdNDP) reveals that the  $\text{Ta}_4\text{B}_{18}$  cluster has  $\sigma$  antiaromaticity and  $\pi$  aromaticity, *i.e.*, a conflicting aromaticity. The simulated photoelectron spectra (PES) of all anionic clusters are also provided for future experimental investigations.

## 1. Introduction

As an adjacent element of carbon (C), boron (B) has three valence electrons ( $2s^2 2p^1$ ), and possesses a diverse and complex range of chemistry. Due to the characteristic of electron deficiency, B aggregates into various structures by sharing electrons and easily forms multicenter-two electron (mc-2e) bonds, which lead to various cluster structures.<sup>1–3</sup> In the past decade, combining experimental and theoretical calculations, it was found that small and medium-sized pure B clusters could have the planar,<sup>4–6</sup> quasi-planar,<sup>7–9</sup> double ring,<sup>10,11</sup> cage-like,<sup>12–15</sup> bilayer,<sup>16,17</sup> and core-shell<sup>18</sup> structures. The  $\text{B}_n^-$  clusters possess the planar or quasi-planar structures form up to the size of  $n \sim 38$ , whereas the neutral counterparts from  $n = 20$  exhibit a transition from the planar to the double-ring tubular shape.<sup>19</sup> The discoveries of planar  $\text{B}_{36}^{0/-}$ ,<sup>9</sup> fullerene-like  $\text{B}_{40}^{0/-}$  (ref. 15) and bilayer  $\text{B}_{48}^{0/-}$  (ref. 17) represent three major breakthroughs in the study of boron clusters. The planar  $\text{B}_{36}$  proves the viability of monolayer boron sheets with hexagonal vacancies, which leads to the concept of borophene. The cage-like  $\text{B}_{40}$  can be regarded as a boron analogue of  $\text{C}_{60}$  (ref. 20) and the bilayer  $\text{B}_{48}$  can be extended to a two-dimensional bilayer phase.<sup>16</sup>

Doping transition-metal (TM) atoms is known as an effective approach to stabilize pure B clusters and to change their geometries and electronic properties. Up to now, the doping of B clusters with different numbers of metal atoms has led to many novel structures, *e.g.* (i) planar molecular wheel,<sup>21–23</sup> (ii) half-sandwich,<sup>24</sup> inverse sandwich<sup>25,26</sup> and inverse triple-

decker<sup>27</sup> clusters, (iii) drum-like structures,<sup>28–30</sup> (iv) the endohedral boron cages,<sup>31–34</sup> and (v) metallo-borospherenes.<sup>35–38</sup>

Doping single TM atom into small-sized B clusters produces perfect TM-centered monocyclic B wheel clusters such as  $\text{Co@B}_8^-$ ,<sup>21</sup>  $\text{Rh@B}_9^-$ ,<sup>22</sup> and  $\text{Ta@B}_{10}^-$ .<sup>23</sup> The 10 coordination number (CN) of  $\text{Ta@B}_{10}^-$  is known as the highest number among the planar species. With the increase of the number of B atoms, the structure growth pattern changes into the half-sandwich structures and the metal-centered B drum structures, such as  $\text{Rh@B}_{12}^-$ ,<sup>24</sup>  $\text{Co@B}_{16}^-$ ,<sup>28</sup>  $\text{Rh@B}_{18}^-$ ,<sup>29</sup> and  $\text{Ta@B}_{20}^-$ .<sup>30</sup> Some highly stable endohedral B cages are also predicted by theoretical calculations, for example,  $\text{Mo@B}_{22}$ ,<sup>32</sup>  $\text{W@B}_{24}$ ,<sup>33</sup> and  $\text{Co@B}_{40}^-$ .<sup>34</sup>

A new class of di-metal-doped inverse sandwich complexes, including  $\text{La}_2\text{B}_7^-$ ,<sup>25</sup>  $\text{Pr}_2\text{B}_8^-$ ,<sup>26</sup> and  $\text{La}_2\text{B}_9^-$ ,<sup>25</sup> have been observed by photoelectron spectra (PES) and density functional theory (DFT) calculations. Because of the unique (d-p) $\delta$  bond between metallic 5d orbitals and  $\text{B}_n$  rings, these lowest energy structures exhibit a higher level of stability than the other isomers. The first icosahedral clusters of  $\text{M}_2\text{B}_{10}$  (M = Rh, Ir)<sup>39</sup> were found in the theoretical investigations. Moreover, the PES results combined with DFT calculations has confirmed that the  $\text{La}_3\text{B}_{14}^-$  cluster has a La–B<sub>8</sub>–La–B<sub>8</sub>–La inverse triple-decker structure, which is used to assemble 1D lanthanide B nanowires.<sup>27</sup> More recently, the first metallo-borospherenes  $\text{La}_3\text{B}_{18}^-$  and  $\text{Tb}_3\text{B}_{18}^-$  ( $D_{3h}$ )<sup>35</sup> were observed in the experiment, and the calculations confirmed that their structures are composed of two  $\text{B}_6$  triangles linked together at their three corners with three  $\text{B}_2$  units. The core-shell spherical trihedral metallo-borospherene  $\text{La}_3\text{&[B}_2\text{@B}_{18}]^-$  (ref. 36) and the smallest metallo-borospherene  $\text{Ta}_3\text{B}_{12}^-$  (ref. 37) were subsequently predicted. Among them, the  $D_{3h}$   $\text{Ta}_3\text{B}_{12}^-$  compound is first metallo-borospherene with  $\sigma + \pi + \delta$  triple aromaticity. The

Key Laboratory of Materials Modification by Laser, Ion and Electron Beams (Dalian University of Technology), Ministry of Education, Dalian 116024, China. E-mail: parksj@dlut.edu.cn

† Electronic supplementary information (ESI) available. See DOI: 10.1039/d1ra02525b



perfect core-shell  $\text{La}_4[\text{B}@\text{B}_4@\text{B}_{24}]^{0/+/-}$  clusters have been theoretically proposed to possess four equivalent inter-connected  $\text{B}_6$  triangles on the cage surface.<sup>38</sup>

In this work, we report the schematic study of the four TM atoms doped  $\text{B}_{18}$  clusters,  $\text{TM}_4\text{B}_{18}^{0/+/-}$  (TM = Hf, Ta, W, Re, Os). These clusters can be thought that they are built up with four TM doped B wheel units by sharing B atoms on their peripheral ring. Among them, the bonding pattern shows this  $\text{Ta}_4\text{B}_{18}$  has 50 skeleton electrons on the cage surface suggesting a spherical aromatic system with filled  $1s + 1p + 1d + 2s + 1f + 2p + 2d$  molecular orbitals. It is also found that the ground-state structure of  $\text{Ta}_4\text{B}_{18}$  shows a conflicting aromaticity.

## 2. Computational methods

The optimization of the lowest energy structures of  $\text{TM}_4\text{B}_{18}^{0/+/-}$  (TM = Hf, Ta, W, Re, Os) were conducted using our developed comprehensive genetic algorithm (CGA) code<sup>40</sup> incorporated with DFT calculations (CGA-DFT). The all-electron method with double- $\zeta$  numerical plus polarization  $d$ -function (DND) basis sets and the Perdew–Burke–Ernzerhof (PBE) functional within the generalized gradient approximation (GGA)<sup>41</sup> were used during each step of CGA using DMol<sup>3</sup> package.<sup>42</sup> Each structure was optimized without any symmetry constraint. The CGA code randomly generated sixteen initial parent configurations for each cluster system. The new structures were created by mating, perturbation, and exchange of the atom type of a pair of different types of atoms.<sup>43</sup> In order to achieve the global minimum of potential energy surface (PES), all cluster systems had at least 3000 iterations.

After the global search of CGA-DFT, the low-energy isomers were more accurately optimized by Gaussian16 program<sup>44</sup> for  $\text{TM}_4\text{B}_{18}^{0/+/-}$  (TM = Hf, Ta, W, Re, Os). The previous studies proved the feasibility of the PBE0 functional<sup>45</sup> to describe the energy differences between different isomers of TM doped B clusters.<sup>35,37,39,46–48</sup> Moreover, our previous study of the single TM

atom doped  $\text{B}_n$  ( $n = 7–10$ ) clusters<sup>49</sup> also confirmed that PBE0 functional can precisely describe the interactions between TM atom and B atom by comparing with the high-level CCSD(T)<sup>50</sup> results. For basis set, the 6-311G\* was proved enough to describe B atom in our study of pure boron clusters.<sup>51</sup> We further calculated the equilibrium bond lengths and vibrational frequencies of TM (TM = Hf, Ta, W, Re, Os) dimer under the different basis sets and found that the def2-TZVP basis set is more suitable for TM atom (see Table S1†). Therefore, PBE0 functional combined with 6-311G\* basis set for B and def2-TZVP basis set for TM atoms were chosen for our systems. Furthermore, chemical bonding analyses were performed using the adaptive natural density partitioning (AdNDP 2.0) program.<sup>52</sup>

## 3. Results and discussion

### 3.1. Lowest energy structures of $\text{TM}_4\text{B}_{18}^{0/+/-}$ (TM = Hf, Ta, W, Re, Os)

The optimized lowest energy structures of neutral  $\text{TM}_4\text{B}_{18}$  (TM = Hf, Ta, W, Re, Os) clusters and corresponding anionic species, along with their point group symmetries with 0.1 Å tolerance, are presented in Fig. 1. More information about the low-lying isomer structures is given in Fig. S1 of the ESI.† The summary of the structural and electronic properties of the ground state in both neutral and anionic series is listed in Table 1. All ground states are found to be singlet or doublet with exception of the  $\text{Re}_4\text{B}_{18}$  cluster, which has the triplet states of spin multiplicity.

As shown in the upper panel of Fig. 1, the lowest energy configuration of the neutral  $\text{Hf}_4\text{B}_{18}$  has  $D_2$  symmetry and it is composed of four twisted umbrella-like  $\text{Hf}@\text{B}_9$  units by sharing the B atoms on their rings. The distances between the Hf atoms are in the range of 3.132 to 3.560 Å, and the average bond length between metal atoms ( $R_{\text{TM-TM}}$ ) is 3.346 Å. The bonding lengths between each Hf atom and its neighboring B atoms are in

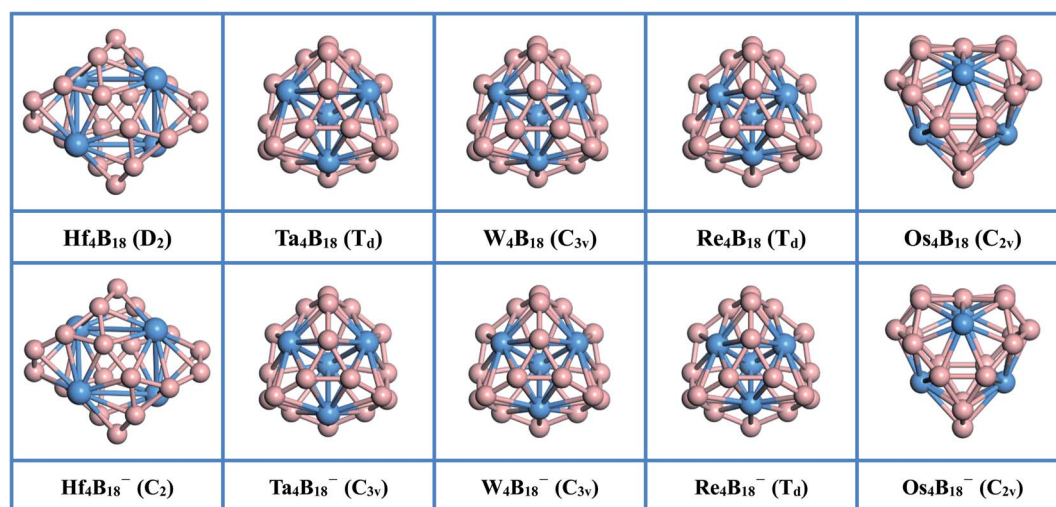


Fig. 1 The lowest energy structures of  $\text{TM}_4\text{B}_{18}$  (TM = Hf, Ta, W, Re, Os) clusters (upper panel) and corresponding anionic clusters (lower panel). The point group symmetry of each cluster is presented in parentheses. The blue and pink spheres are TM and B, respectively.



**Table 1** The structural and electronic properties of  $\text{TM}_4\text{B}_{18}^{0/-}$  (TM = Hf, Ta, W, Re, Os) clusters. The minimum and maximum distances between TM atoms, between TM and B, and between B atoms are shown with their average distance values ( $R_{\text{TM-TM}}$ ,  $R_{\text{TM-B}}$ , and  $R_{\text{B-B}}$ , respectively in Å). The average charge transfer the TM atom to the B cage ( $Q_{\text{TM}}$ , in |e|), binding energies per atom ( $E_{\text{b}}$ , in eV), HOMO–LUMO energy gap ( $E_{\text{HL}}$ , in eV), and the lowest vibrational frequency ( $\omega_{\text{min}}$ , in  $\text{cm}^{-1}$ ) are also presented

	Min–Max ( $R_{\text{TM-TM}}$ )	Min–Max ( $R_{\text{TM-B}}$ )	Min–Max ( $R_{\text{B-B}}$ )	$Q_{\text{TM}}$	$E_{\text{b}}$	$E_{\text{HL}}$	$\omega_{\text{min}}$
$\text{Hf}_4\text{B}_{18} (D_2)$	3.132–3.560 (3.346)	2.378–2.458 (2.419)	1.533–1.783 (1.635)	1.148	5.80	2.60	120.33
$\text{Hf}_4\text{B}_{18}^- (C_2)$	3.106–3.541 (3.324)	2.379–2.468 (2.421)	1.537–1.792 (1.640)	1.007	5.89	1.54	64.17
$\text{Ta}_4\text{B}_{18} (T_d)$	3.011 (3.011)	2.351–2.358 (2.353)	1.565–1.697 (1.631)	0.487	6.02	2.61	158.80
$\text{Ta}_4\text{B}_{18}^- (C_{3v})$	2.946–3.073 (3.010)	2.332–2.378 (2.358)	1.565–1.701 (1.634)	0.383	6.13	1.70	121.59
$\text{W}_4\text{B}_{18} (C_{3v})$	2.609–2.912 (2.761)	2.294–2.365 (2.333)	1.555–1.720 (1.629)	0.068	6.16	2.41	136.90
$\text{W}_4\text{B}_{18}^- (C_{3v})$	2.666–2.831 (2.749)	2.315–2.352 (2.332)	1.562–1.706 (1.629)	−0.042	6.30	1.87	126.07
$\text{Re}_4\text{B}_{18} (T_d)$	2.571–2.574 (2.573)	2.298–2.359 (2.319)	1.568–1.694 (1.629)	−0.166	6.10	1.85	216.66
$\text{Re}_4\text{B}_{18}^- (T_d)$	2.541–2.561 (2.554)	2.289–2.391 (2.326)	1.570–1.712 (1.639)	−0.189	6.26	1.37	153.41
$\text{Os}_4\text{B}_{18} (C_{2v})$	—	2.104–2.250 (2.170)	1.564–1.766 (1.681)	−0.089	5.95	1.69	102.89
$\text{Os}_4\text{B}_{18}^- (C_{2v})$	—	2.108–2.278 (2.170)	1.576–1.759 (1.687)	−0.190	6.09	1.55	111.05

between 2.378 and 2.458 Å, and the average bond length between metal atom and B ( $R_{\text{TM-B}}$ ) is 2.419 Å. The distances between B atoms are in between 1.533 and 1.783 Å, which smallest value is slightly shorter than the B=B double bond (1.56 Å)<sup>53</sup> and the largest value is longer than the typical B–B single bond (1.70 Å).<sup>53</sup> Besides, the natural population analysis (NPA) shows that each Hf serves as the donor of 1.148 |e| to the  $\text{B}_{18}$  skeleton, implying the formation of typical charge-transfer  $\text{Hf}_4^{4+}\text{B}_{18}^{4-}$  complexes.

The  $\text{Ta}_4\text{B}_{18}$  forms a structure with the highly-symmetric point group of  $T_d$  with the electronic state of  $^1A_1$ . The  $\text{Ta}_4\text{B}_{18}$  is composed of the previously reported the four planar molecular  $\text{Ta@B}_9$  wheels<sup>47</sup> by sharing the B atoms on the rings. The total energy of this structure is much lower than the second low-lying isomers ( $C_2$ ) by 1.114 eV at the levels of PBE0/TZVP (see Fig. S1†). The interatomic distance between Ta atoms is 3.011 Å. The bonding lengths between each Ta atom and B atoms are in the range of 2.351 to 2.358 Å, which are slightly shorter than those in the freestanding  $\text{Ta@B}_9$  (2.39 Å),<sup>47</sup> and the lengths between adjacent B atoms (1.565–1.697 Å) are longer than  $\text{Ta@B}_9$  (1.54 Å)<sup>47</sup> at the PBE0 levels, suggesting that doping more Ta atom weakens the interaction between B atoms and strengthen the Ta and B bonding. The  $\text{Ta}_4\text{B}_{18}$  also can be regarded as the  $\text{Ta}_4$  cluster in the middle bonded with the B atoms. We found that the lowest energy structure of  $\text{Ta}_4$  cluster has a tetrahedral structure with  $T_d$  symmetry and its bonding length is 2.541 Å, which is significantly shorter than that of  $\text{Ta}_4$  moiety (3.011 Å) in  $\text{Ta}_4\text{B}_{18}$ . It shows that the strong interaction between Ta and B atoms weakens the bonding strength between Ta atoms, resulting in longer lengths. Moreover, NPA shows each Ta atom donates 0.487 |e| to the  $\text{B}_{18}$  skeleton forming a covalent bond due to the larger B electronegativity.

For the lowest energy structures of  $\text{W}_4\text{B}_{18}$  and  $\text{Re}_4\text{B}_{18}$ , their geometric configurations are very similar to the  $\text{Ta}_4\text{B}_{18}$  cluster. Doping Re atoms into the  $\text{B}_{18}$  framework leads to a magnetic cluster  $\text{Re}_4\text{B}_{18}$  ( $T_d$ ) with the triplet states of spin multiplicity. The influence of atomic radius and magnetic moment makes it have a higher symmetry than  $\text{W}_4\text{B}_{18}$  ( $C_{3v}$ ). The average distances of  $\text{W}_4\text{B}_{18}$  between W atoms ( $R_{\text{TM-TM}}$ ), and between W and B

atoms ( $R_{\text{TM-B}}$ ), are 2.761 and 2.333 Å, respectively. For the  $\text{Re}_4\text{B}_{18}$  cluster, the  $R_{\text{TM-TM}}$  and  $R_{\text{TM-B}}$  are 2.573 Å and 2.319 Å, respectively. It can be seen that  $R_{\text{TM-TM}}$  and  $R_{\text{TM-B}}$  of the  $\text{Re}_4\text{B}_{18}$  cluster are shorter than those of the  $\text{W}_4\text{B}_{18}$  cluster, but the average bond length between B atoms ( $R_{\text{B-B}}$ ) is the same (1.629 Å). For  $\text{Re}_4\text{B}_{18}$ , compared with the previously reported planar molecular wheel  $\text{Re@B}_9$ ,<sup>54</sup> we find that the bonding length of  $\text{Re}_4\text{B}_{18}$  (1.568–1.694 Å) between adjacent B atoms are longer than the  $\text{Re@B}_9$  (1.543–1.571 Å) at the PBE0 levels.

The optimized structure of  $\text{Os}_4\text{B}_{18}$  is a hollow cage-like structure with  $C_{2v}$  symmetry, which is very different from the other  $\text{TM}_4\text{B}_{18}$  (TM = Hf, Ta, W, Re) clusters. The  $\text{Os}_4\text{B}_{18}$  is insufficient to support the large spherical B skeleton due to the further reduction of metal atomic radius. Therefore, the lowest energy structure of cage-like  $\text{Os}_4\text{B}_{18}$  is assembled by two types of planar molecular wheels of  $\text{Os@B}_7$  and  $\text{Os@B}_8$ , and the Os atoms on cage surface with the coordination numbers (CN) are 7 and 8. Moreover, the bonding length between B atoms are in the range of 1.564 to 1.766 Å, and the average ( $R_{\text{B-B}}$ ) is 1.681 Å, which is very close to the single bond value. The bonding lengths between each Os atom and its neighboring B atom are in the range of 2.104–2.250 Å, and the  $R_{\text{TM-B}}$  is 2.170 Å. It can be seen from Table 1 that the average distance between Os and B atoms ( $R_{\text{TM-B}}$ ) becomes shorter rapidly when the size of metal atom decreases, which leads to a tighter bond between the TM and B atom. The coordinates of the lowest energy structures of  $\text{TM}_4\text{B}_{18}$  (TM = Hf, Ta, W, Re, Os) are listed in Table S2 of the ESI.†

All corresponding global minima of anionic clusters are exhibited in the lower panel of Fig. 1. The geometric structures of  $\text{TM}_4\text{B}_{18}^-$  (TM = Hf, Ta, W, Re, Os) are very similar to their corresponding neutral clusters. However, owing to the Jahn–Teller effect, the capture of one additional electron results in the low point group symmetries for Hf and Ta. The lowest energy structure of  $\text{Hf}_4\text{B}_{18}^-$  has  $C_2$  symmetry, and each Hf atom transfers fewer electrons (1.007 |e|) to the  $\text{B}_{18}$  skeleton than the neutral. The structures of  $\text{TM}_4\text{B}_{18}^-$  (TM = Ta, W, Re) are very similar like the neutral ones and consist of planar molecular wheels of the  $\text{TM@B}_9$  unit. However, compared with the



corresponding neutral clusters, their  $R_{\text{TM-TM}}$  is shorter and  $R_{\text{B-B}}$  is slightly longer. NPA shows each TM atom donates electrons to the  $\text{B}_{18}$  skeleton in the range of  $-0.189$  |e| to  $0.383$  |e|, which forms the typical covalent bonds. The structure of  $\text{Os}_4\text{B}_{18}^-$  ( $C_{2v}$ ) is also a hollow cage-like structure, its  $R_{\text{TM-B}}$  and  $R_{\text{B-B}}$  are little changed. The coordinates of all anionic clusters are listed in Table S3 of the ESI.† The  $\text{TM}_4\text{B}_{18}^{0/-}$  (TM = Hf, Ta, W, Re, Os) clusters can be thought that they are constructed with four TM doped B wheel units by sharing B atoms. This approach could be a new pathway to produce various TM doped B cluster structures.

To gain a better understanding of the stability of these nanoclusters, we further examined the electronic properties. The binding energies per atom ( $E_b$ ) is regarded as an effective parameter to evaluate the thermodynamic stability of a cluster, which is calculated by

$$E_b = (4E_{\text{TM}} + 18E_{\text{B}} - E_{\text{TM}_4\text{B}_{18}}^{0/-})/22 \quad (1)$$

In the eqn (1),  $E_{\text{TM}_4\text{B}_{18}}^{0/-}$ ,  $E_{\text{TM}}$  and  $E_{\text{B}}$  represent the total energy of  $\text{TM}_4\text{B}_{18}^{0/-}$  (TM = Hf, Ta, W, Re, Os) clusters, a TM atom, and a B atom, respectively. Here, the larger  $E_b$  value implies the more favorable thermodynamic stability of a cluster. In neutral clusters, the  $\text{W}_4\text{B}_{18}$  has a maximum  $E_b$  value of 6.16 eV, while the  $\text{Hf}_4\text{B}_{18}$  has a minimum  $E_b$  value (5.80 eV). The  $E_b$  values of  $\text{TM}_4\text{B}_{18}$  (Ta, W, Re) are larger than those of others, so these clusters have a higher thermodynamic stability. The same trend is observed for the corresponding anions. As a reflection of the energy cost for an electron jumping from the highest occupied molecular orbital (HOMO) to the lowest unoccupied molecular orbital (LUMO), the HOMO–LUMO energy gap ( $E_{\text{HL}}$ ) can reveal the chemical stability of a cluster. In comparison with cage-like  $\text{Ta}_3\text{B}_{12}^-$  which possess a  $E_{\text{HL}}$  of 2.50 eV with three equivalent  $\text{Ta@B}_8$  octagons sharing two eclipsed  $\text{B}_3$  triangles at the top and bottom interconnected by three  $\text{B}_2$  units on the waist,<sup>37</sup> the lowest energy structures of  $\text{Hf}_4\text{B}_{18}$  and  $\text{Ta}_4\text{B}_{18}$  possess a large  $E_{\text{HL}}$  of 2.60 and 2.61 eV, respectively, being less chemically reactive than others. For all anionic clusters, due to the trapping of an electron, the  $E_{\text{HL}}$  of these species is decreased and significantly less than the neutral clusters. Among them, the  $\text{W}_4\text{B}_{18}^-$  cluster has the largest  $E_{\text{HL}}$  value of 1.87 eV, while the  $E_{\text{HL}}$  of the  $\text{Re}_4\text{B}_{18}^-$  cluster is the smallest, only 1.37 eV. Moreover, vibrational frequency calculations confirm that there are no imaginary frequencies for all these ground-state structures, and the corresponding lowest frequencies are listed in Table 1.

### 3.2. Bonding analysis

The structural and electronic properties of  $\text{TM}_4\text{B}_{18}^{0/-}$  (TM = Hf, Ta, W, Re, Os) nanoclusters shows that the neutral  $\text{Ta}_4\text{B}_{18}$  and  $\text{Hf}_4\text{B}_{18}$  clusters are chemically more inert than the others (larger  $E_{\text{HL}}$ )<sup>55</sup> but relatively the  $\text{Ta}_4\text{B}_{18}$  has larger  $E_b$  (thermodynamically more stable)<sup>56</sup> than  $\text{Hf}_4\text{B}_{18}$ . Based on this analysis, we further investigate the bonding properties of the  $\text{Ta}_4\text{B}_{18}$  cluster. The molecular orbital (MO) energy-level diagram and the relevant MOs of  $\text{Ta}_4\text{B}_{18}$  derived from the  $\text{Ta}_4$  moiety and  $\text{B}_{18}$  skeleton, which is presented in Fig. 2. It shows the interactions between

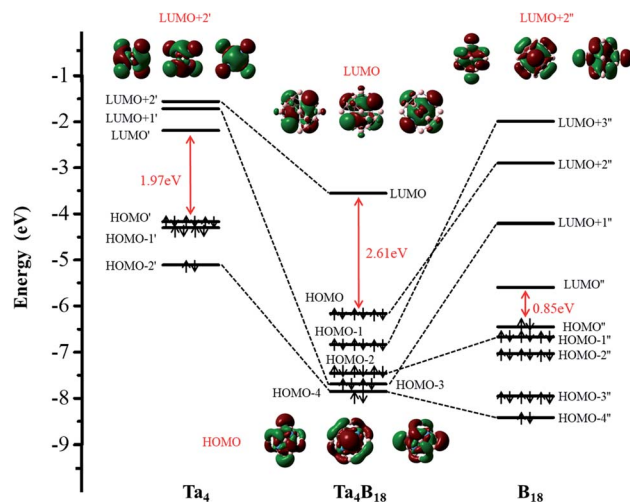


Fig. 2 The Kohn–Sham molecular orbital correlation diagram for  $\text{Ta}_4\text{B}_{18}$ . It shows the interactions between the orbitals of the  $\text{Ta}_4$  atoms and the group orbitals of the  $\text{B}_{18}$  skeleton.

the orbitals of the four Ta atoms and the group orbitals of the  $\text{B}_{18}$  skeleton. Among them, LUMO, HOMO and HOMO –  $n$  represent the energy-levels of the  $\text{Ta}_4\text{B}_{18}$  cluster, respectively. LUMO', LUMO +  $n'$ , HOMO' and HOMO –  $n'$  represent the energy-levels of  $\text{Ta}_4$  moiety. LUMO'', LUMO +  $n''$ , HOMO'' and HOMO –  $n''$  represent the energy-levels of the  $\text{B}_{18}$  skeleton. Since the global minimum of  $\text{B}_{18}$  is a planar structure, the stabilization of the 3D  $\text{B}_{18}$  framework is entirely due to its strong bonding with the  $\text{Ta}_4$  moiety. The 3D  $\text{B}_{18}$  skeleton has a small HOMO–LUMO gap of 0.85 eV. The addition of four Ta atoms results in a closed-shell  $\text{Ta}_4\text{B}_{18}$  with a large HOMO–LUMO gap of 2.61 eV. It is noted that the  $T_d$  symmetry of  $\text{Ta}_4\text{B}_{18}$  leads to the feature level of LUMO, HOMO, HOMO – 1 and HOMO – 2 are triple degenerates. Furthermore, we find that the LUMO + 2' of  $\text{Ta}_4$  moiety is unoccupied and mainly becomes the LUMO orbital of  $\text{Ta}_4\text{B}_{18}$ . For the occupied MOs of  $\text{Ta}_4\text{B}_{18}$ , HOMO, HOMO – 1 and HOMO – 2 are formed from LUMO + 2'' ( $\sigma$  orbitals), LUMO + 3'' ( $\sigma$  orbitals), and HOMO – 1'' ( $\pi$  orbitals) of  $\text{B}_{18}$  framework, respectively. The HOMO – 3 is a  $\sigma + \pi$  hybrid orbital, which derives from the mixing of LUMO + 1' ( $\pi$  orbit) with LUMO + 1'' ( $\sigma$  orbit). The HOMO – 4 of  $\sigma + \sigma$  hybrid orbital is formed from two  $\sigma$  orbit of HOMO – 2' and HOMO – 4'. Moreover, the Ta atom in  $\text{Ta}_4\text{B}_{18}$  has total on-site Wiberg bond order (WBO) of 5.82, which well supporting the spherical coordination interactions between  $\text{Ta}_4$  moiety and  $\text{B}_{18}$  skeleton.

We also performed a chemical bonding analysis of the spherical  $\text{Ta}_4\text{B}_{18}$  using the AdNDP method. As depicted in Fig. 3, the  $\text{Ta}_4\text{B}_{18}$  cluster contains 12 localized bonds and 25 delocalized bonds, ordered by occupation number (ON) ranging from 1.80 |e| to 2.00 |e|. The 12 localized B–B bonds are all 2c–2e  $\sigma$  bonds on the peripheral edge of the  $\text{B}_{18}$  skeleton, which are mainly composed of B 2s/2p electrons, and their ONs are 1.80 |e|. Among the 25 delocalized bonds, there are 4 equivalent 3c–2e  $\sigma$  bonds on the  $\text{B}_3$  triangles (ON = 1.85 |e|). The three sets of the delocalized 10c–2e Ta– $\text{B}_9$  bonds (ON = 1.88–1.90 |e|) over the boron skeleton, which includes 4 equivalent Ta ( $d_{x^2-y^2}$ )– $\text{B}_9$





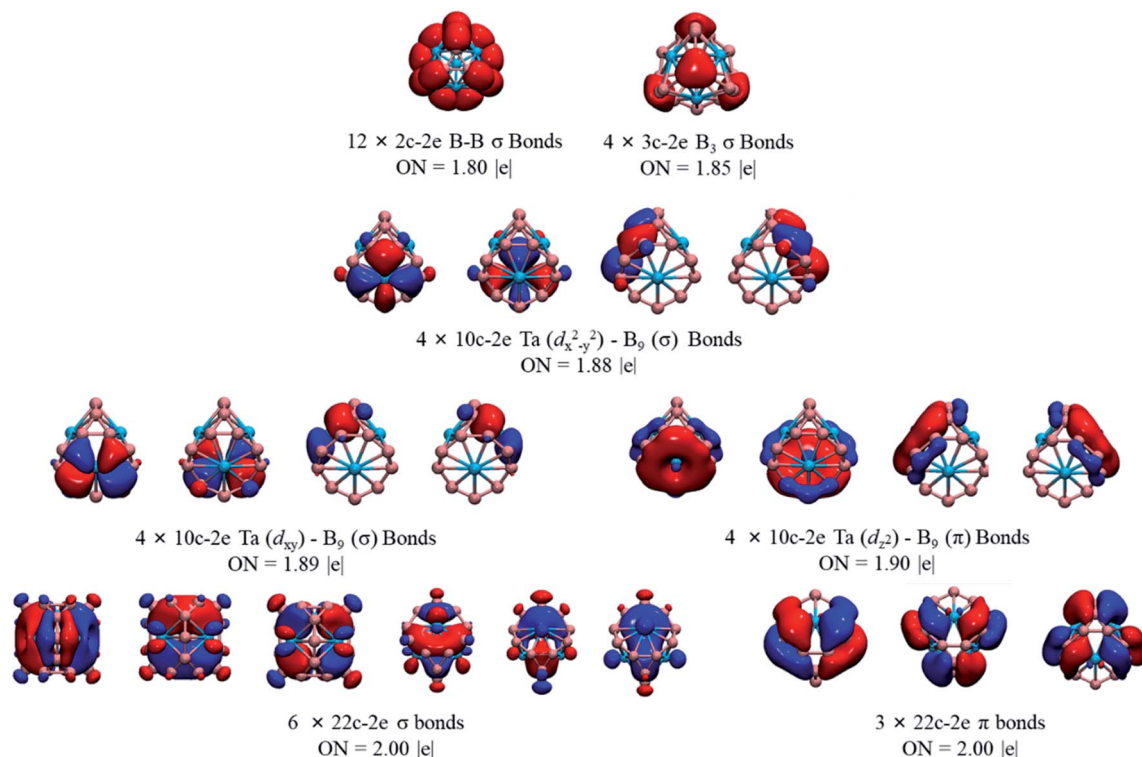


Fig. 3 AdNDP bonding patterns of Ta<sub>4</sub>B<sub>18</sub>, with the occupation numbers (ON).

( $\sigma$ ) bonds, 4 equivalent Ta ( $d_{xy}$ )-B<sub>9</sub> ( $\sigma$ ) bonds, and 4 equivalent Ta ( $d_{z^2}$ )-B<sub>9</sub> ( $\pi$ ) bonds. As shown in the bottom row of Fig. 3, there are 9 totally delocalized 22c-2e bonds distributed on the entire spherical skeleton with ON = 2.00 |e|. Among them, 6 are  $\sigma$  and the other 3 are  $\pi$  bonds. Therefore, the Ta<sub>4</sub>B<sub>18</sub> cluster has 10 delocalized  $\sigma$  bonds in total (4 equivalent 3c-2e  $\sigma$  bonds plus 6 equivalent 22c-2e bonds), leading to the  $\sigma$  antiaromaticity according to  $4n$  ( $n = 5$ ) Hückel's rule. Meanwhile, the 3 totally

delocalized  $\pi$ -bonds (22c-2e bonds) satisfies the Hückel rules of  $4n + 2$  ( $n = 1$ ) of  $\pi$  aromaticity. Thus, Ta<sub>4</sub>B<sub>18</sub> is a conflicting aromatic system with 20  $\sigma$  and 6  $\pi$  totally delocalized electrons. Note that 50 skeletal electrons are distributed on the cage surface is a magic number for a closed-shell three-dimensional spherical structure in which the 25 delocalized orbitals are completely filled with electron pairs leading to a closed-shell  $1S^21P^61D^{10}2S^21F^{14}2P^62D^{10}$  configuration.

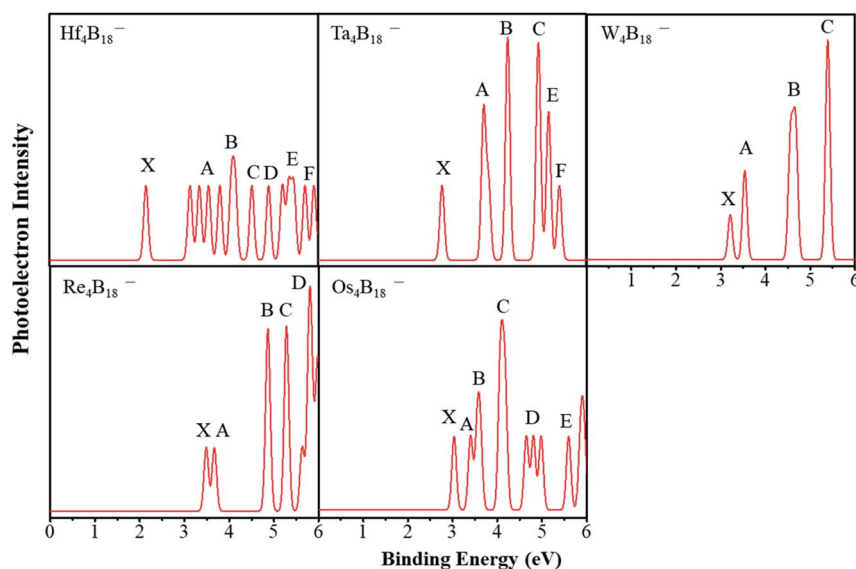


Fig. 4 The simulated photoelectron spectra of TM<sub>4</sub>B<sub>18</sub><sup>−</sup> (TM = Hf, Ta, W, Re, Os) clusters.

### 3.3. Simulated photoelectron spectra of $\text{TM}_4\text{B}_{18}^-$ (TM = Hf, Ta, W, Re, Os)

Photoelectron spectra (PES) can be used as the fingerprints about the electronic structures of nanoclusters. Therefore, we simulated the PES of  $\text{TM}_4\text{B}_{18}^-$  (TM = Hf, Ta, W, Re, Os) anionic clusters, hoping to help experimentally determine these lowest energy structures.

First, we consider the simulated PES of  $\text{Ta}_4\text{B}_{18}^-$  and  $\text{Re}_4\text{B}_{18}^-$  by comparing with the experimentally reported of  $\text{Ta@B}_9^-$  and  $\text{Re@B}_9^-$ . As displayed in Fig. 4, the spectral features are labeled X, A, B, etc. In each spectrum, the X peak represents the vertical detachment energy (VDE) which denotes the transition from the anionic ground-state to the neutral ground-state, and the other (A, B, etc.) peaks indicate transitions to the excited state of the neutral complexes. The VDE of  $\text{Ta}_4\text{B}_{18}^-$  is approximately 2.77 eV. After this first peak, there are five peaks between 3.5 eV and 5.5 eV. In the experimental spectrum of  $\text{Ta@B}_9^-$ , the first X peak is located at around 3.64 eV,<sup>47</sup> indicating the structure of  $\text{Ta}_4\text{B}_{18}^-$  assembled by  $\text{Ta@B}_9^-$  has the lower electron binding energy. For the simulated spectrum of  $\text{Re}_4\text{B}_{18}^-$ , the first two peaks are somewhat weak and close each other. The experimental PES of  $\text{Re@B}_9^-$  also shows two close peaks at 4.02 eV and 4.34 eV,<sup>54</sup> respectively. These lower binding energies of  $\text{Re}_4\text{B}_{18}^-$  are similar to those of  $\text{Ta}_4\text{B}_{18}^-$  by comparison with the experimental results. Presumably, this is caused by the interaction between planar molecular unit wheels ( $\text{Ta@B}_9$  and  $\text{Re@B}_9$ ).

The PES of  $\text{Hf}_4\text{B}_{18}^-$  is simulated and shows a compact spectral pattern, and the first peak is approximately 2.16 eV, following by four consecutive peaks of the same intensity. There are four major peaks (X, A, B and C) of the simulated spectrum of  $\text{W}_4\text{B}_{18}^-$ , and the VDE is approximately 3.19 eV. The simulated spectrum of  $\text{Os}_4\text{B}_{18}^-$  also presents a compact spectral pattern with a VDE of 3.02 eV. To provide detailed data for the future experiment, we further calculated the vertical ionization potentials (VIP) and vertical electron affinities of neutral clusters, and adiabatic detachment energy (ADE) of anionic clusters, which are shown in Table 2. The  $\text{W}_4\text{B}_{18}$  shows a larger VIP value

(7.52 eV) and VEA value (2.82 eV) than others. The  $\text{Re}_4\text{B}_{18}$  shows a larger ADE value of 3.07 eV than others. However, the spherical  $\text{Ta}_4\text{B}_{18}$  has a large VIP value (7.37 eV) and a moderate VEA value (2.46 eV).

## 4. Conclusion

We carried out unbiased search for the lowest energy structures of  $\text{TM}_4\text{B}_{18}^{0/-}$  clusters (TM = Hf, Ta, W, Re, Os). The structural analysis shows that they are composed of the four planar molecular  $\text{TM@B}_9$  wheel units sharing the B atoms except for  $\text{Os}_4\text{B}_{18}^{0/-}$ , which has a hollow cage-like structure assembled by two types of planar molecular wheels of  $\text{Os@B}_7$  and  $\text{Os@B}_8$  due to the reduction of the atomic radius. According the electronic properties, spherical  $\text{Ta}_4\text{B}_{18}$  has large  $E_b$  and  $E_{\text{HL}}$ . The chemical bonding analyses showed that it has the  $\sigma$  antiaromaticity with  $4n$  ( $n = 5$ ) and  $\pi$  aromaticity with  $4n + 2$  ( $n = 1$ ) from Hückel's rule, resulting in a conflicting aromatic system. Finally, the PES of all anionic clusters was simulated which provides predictive information for future experimental investigations.

## Conflicts of interest

There are no conflicts to declare.

## Acknowledgements

This work was supported by the Research Funds for the Central Universities of China (DUT20RC(5)014), and the Supercomputing Center of Dalian University of Technology.

## References

- 1 A. I. Boldyrev and L.-S. Wang, *Phys. Chem. Chem. Phys.*, 2016, **18**, 11589–11605.
- 2 J. Zhao, Q. Du, S. Zhou and V. Kumar, *Chem. Rev.*, 2020, **120**, 9021–9163.
- 3 D. Li, J. Gao, P. Cheng, J. He, Y. Yin, Y. Hu, L. Chen, Y. Cheng and J. Zhao, *Adv. Funct. Mater.*, 2020, **30**, 1904349.
- 4 H.-J. Zhai, A. N. Alexandrova, K. A. Birch, A. I. Boldyrev and L. Wang, *Angew. Chem., Int. Ed.*, 2003, **42**, 6004–6008.
- 5 A. P. Sergeeva, D. Y. Zubarev, H.-J. Zhai, A. I. Boldyrev and L.-S. Wang, *J. Am. Chem. Soc.*, 2008, **130**, 7244–7246.
- 6 W. Huang, A. P. Sergeeva, H.-J. Zhai, B. B. Averkiev, L.-S. Wang and A. I. Boldyrev, *Nat. Chem.*, 2010, **2**, 202–206.
- 7 W.-L. Li, Y.-F. Zhao, H.-S. Hu, J. Li and L.-S. Wang, *Angew. Chem., Int. Ed.*, 2014, **126**, 5646–5651.
- 8 W.-L. Li, Q. Chen, W.-J. Tian, H. Bai, Y.-F. Zhao, H.-S. Hu, J. Li, H.-J. Zhai, S.-D. Li and L.-S. Wang, *J. Am. Chem. Soc.*, 2014, **136**, 12257–12260.
- 9 Z. A. Piazza, H.-S. Hu, W.-L. Li, Y.-F. Zhao, J. Li and L.-S. Wang, *Nat. Commun.*, 2014, **5**, 3113.
- 10 B. Kiran, S. Bulusu, H.-J. Zhai, S. Yoo, X. C. Zeng and L.-S. Wang, *Proc. Natl. Acad. Sci. U. S. A.*, 2005, **102**, 961–964.
- 11 X. Wu, L. Sai, S. Zhou, P. Zhou, M. Chen, M. Springborg and J. Zhao, *Phys. Chem. Chem. Phys.*, 2020, **22**, 12959–12966.

**Table 2** Vertical ionization potentials (VIP), vertical electron affinities (VEA), vertical detachment energy (VDE), and adiabatic detachment energy (ADE) of  $\text{TM}_4\text{B}_{18}^{0/-}$  (TM = Hf, Ta, W, Re, Os) clusters. All energies are in eV

	VIP <sup>a</sup>	VEA <sup>b</sup>		VDE <sup>c</sup>	ADE <sup>d</sup>
$\text{Hf}_4\text{B}_{18} (D_2)$	6.65	1.53	$\text{Hf}_4\text{B}_{18}^- (C_2)$	2.16	1.88
$\text{Ta}_4\text{B}_{18} (T_d)$	7.37	2.46	$\text{Ta}_4\text{B}_{18}^- (C_{3v})$	2.77	2.65
$\text{W}_4\text{B}_{18} (C_{3v})$	7.52	2.82	$\text{W}_4\text{B}_{18}^- (C_{3v})$	3.19	3.01
$\text{Re}_4\text{B}_{18} (T_d)$	7.25	2.13	$\text{Re}_4\text{B}_{18}^- (T_d)$	3.49	3.07
$\text{Os}_4\text{B}_{18} (C_{2v})$	6.77	2.90	$\text{Os}_4\text{B}_{18}^- (C_{2v})$	3.02	2.97

<sup>a</sup> Vertical ionization energy from the ground state of the neutral to the ground state of the cation. <sup>b</sup> Vertical electronic affinity from the ground state of the neutral to the ground state of the anion. <sup>c</sup> Vertical detachment energy from the ground state of the anion to the ground state of the neutral. <sup>d</sup> Adiabatic detachment energy from the ground state of the anion to the ground state of the neutral.



- 12 J. Zhao, X. Huang, R. Shi, H. Liu, Y. Su and R. B. King, *Nanoscale*, 2015, **7**, 15086–15090.
- 13 Y.-J. Wang, Y.-F. Zhao, W.-L. Li, T. Jian, Q. Chen, X.-R. You, T. Ou, X.-Y. Zhao, H.-J. Zhai, S.-D. Li, J. Li and L.-S. Wang, *J. Chem. Phys.*, 2016, **144**, 064307.
- 14 J. Lv, Y. Wang, L. Zhu and Y. Ma, *Nanoscale*, 2014, **6**, 11692–11696.
- 15 H.-J. Zhai, Y.-F. Zhao, W.-L. Li, Q. Chen, H. Bai, H.-S. Hu, Z. A. Piazza, W.-J. Tian, H.-G. Lu, Y.-B. Wu, Y.-W. Mu, G.-F. Wei, Z.-P. Liu, J. Li, S.-D. Li and L.-S. Wang, *Nat. Chem.*, 2014, **6**, 727–731.
- 16 L. Sai, X. Wu, N. Gao, J. Zhao and R. B. King, *Nanoscale*, 2017, **9**, 13905–13909.
- 17 W.-J. Chen, Y.-Y. Ma, T.-T. Chen, M.-Z. Ao, D.-F. Yuan, Q. Chen, X.-X. Tian, Y.-W. Mu, S.-D. Li and L.-S. Wang, *Nanoscale*, 2021, **13**, 3868–3876.
- 18 J. Zhao, L. Wang, F. Li and Z. Chen, *J. Phys. Chem. A*, 2010, **114**, 9969–9972.
- 19 T. Jian, X. Chen, S.-D. Li, A. I. Boldyrev, J. Li and L.-S. Wang, *Chem. Soc. Rev.*, 2019, **48**, 3550–3591.
- 20 H. W. Kroto, J. R. Heath, S. C. O'Brien, R. F. Curl and R. E. Smalley, *Nature*, 1985, **318**, 162–163.
- 21 C. Romanescu, T. R. Galeev, W.-L. Li, A. I. Boldyrev and L.-S. Wang, *Angew. Chem., Int. Ed.*, 2011, **50**, 9334–9337.
- 22 W.-L. Li, C. Romanescu, T. R. Galeev, Z. A. Piazza, A. I. Boldyrev and L.-S. Wang, *J. Am. Chem. Soc.*, 2012, **134**, 165–168.
- 23 C. Romanescu, T. R. Galeev, W.-L. Li, A. I. Boldyrev and L.-S. Wang, *Acc. Chem. Res.*, 2013, **46**, 350–358.
- 24 I. A. Popov, W.-L. Li, Z. A. Piazza, A. I. Boldyrev and L.-S. Wang, *J. Phys. Chem. A*, 2014, **118**, 8098–8105.
- 25 T.-T. Chen, W.-L. Li, J. Li and L.-S. Wang, *Chem. Sci.*, 2019, **10**, 2534–2542.
- 26 W.-L. Li, T.-T. Chen, D.-H. Xing, X. Chen, J. Li and L.-S. Wang, *Proc. Natl. Acad. Sci. U. S. A.*, 2018, **115**, E6972–E6977.
- 27 T.-T. Chen, W.-L. Li, W.-J. Chen, J. Li and L.-S. Wang, *Chem. Commun.*, 2019, **55**, 7864–7867.
- 28 I. A. Popov, T. Jian, G. V. Lopez, A. I. Boldyrev and L.-S. Wang, *Nat. Commun.*, 2015, **6**, 8654.
- 29 T. Jian, W.-L. Li, X. Chen, T.-T. Chen, G. V. Lopez, J. Li and L.-S. Wang, *Chem. Sci.*, 2016, **7**, 7020–7027.
- 30 W.-L. Li, T. Jian, X. Chen, H.-R. Li, T.-T. Chen, X.-M. Luo, S.-D. Li, J. Li and L.-S. Wang, *Chem. Commun.*, 2017, **53**, 1587–1590.
- 31 P. Jin, Q. Hou, C. Tang and Z. Chen, *Theor. Chem. Acc.*, 2015, **134**, 13.
- 32 Y. Wang, X. Wu and J. Zhao, *J. Cluster Sci.*, 2018, **29**, 847–852.
- 33 J. Lv, Y. Wang, L. Zhang, H. Lin, J. Zhao and Y. Ma, *Nanoscale*, 2015, **7**, 10482–10489.
- 34 J. Liu, Y. Zhang, C. Li, W. Jin, G. Lefkidis and W. Hübner, *Phys. Rev. B*, 2020, **102**, 024416.
- 35 T.-T. Chen, W.-L. Li, W.-J. Chen, X.-H. Yu, X.-R. Dong, J. Li and L.-S. Wang, *Nat. Commun.*, 2020, **11**, 2766.
- 36 X.-Y. Zhao, M. Yan, Z. Wei and S.-D. Li, *RSC Adv.*, 2020, **10**, 34225–34230.
- 37 Y. Zhang, X.-Y. Zhao, M. Yan and S.-D. Li, *RSC Adv.*, 2020, **10**, 29320–29325.
- 38 X.-Q. Lu, C.-Y. Gao, Z. Wei and S.-D. Li, *J. Mol. Model.*, 2021, **27**, 130.
- 39 W.-y. Liang, J. Barroso, S. Jalife, M. a. Orozco-Ic, X. Zarate, X. Dong, Z.-h. Cui and G. Merino, *Chem. Commun.*, 2019, **55**, 7490–7493.
- 40 J. Zhao, R. Shi, L. Sai, X. Huang and Y. Su, *Mol. Simul.*, 2016, **42**, 809–819.
- 41 J. P. Perdew, K. Burke and M. Ernzerhof, *Phys. Rev. Lett.*, 1996, **77**, 3865–3868.
- 42 B. Delley, *J. Chem. Phys.*, 2000, **113**, 7756–7764.
- 43 L. Sai, L. Tang, J. Zhao, J. Wang and V. Kumar, *J. Chem. Phys.*, 2011, **135**, 184305.
- 44 M. Frisch, G. Trucks, H. Schlegel, G. Scuseria, M. Robb, J. Cheeseman, G. Scalmani, V. Barone, G. Petersson and H. Nakatsuji, *Gaussian 16, Revision A. 03*, Gaussian, Inc., Wallingford CT, 2016.
- 45 C. Adamo and V. Barone, *J. Chem. Phys.*, 1999, **110**, 6158–6170.
- 46 W.-L. Li, A. S. Ivanov, J. Federic, C. Romanescu, I. Cernušák, A. I. Boldyrev and L.-S. Wang, *J. Chem. Phys.*, 2013, **139**, 104312.
- 47 C. Romanescu, T. R. Galeev, W.-L. Li, A. I. Boldyrev and L.-S. Wang, *J. Chem. Phys.*, 2013, **138**, 134315.
- 48 B. L. Chen, W. G. Sun, X. Y. Kuang, C. Lu, X. X. Xia, H. X. Shi and G. Maroulis, *Inorg. Chem.*, 2018, **57**, 343–350.
- 49 X. Wu, Y. Wang, X. Zhao, S. Zhou, S. Li, M. Chen and J. Zhao, *Eur. Phys. J. Plus*, 2021, **136**, 328.
- 50 G. D. Purvis and R. J. Bartlett, *J. Chem. Phys.*, 1982, **76**, 1910.
- 51 F. Li, P. Jin, D.-e. Jiang, L. Wang, S. B. Zhang, J. Zhao and Z. Chen, *J. Chem. Phys.*, 2012, **136**, 074302.
- 52 N. V. Tkachenko and A. I. Boldyrev, *Phys. Chem. Chem. Phys.*, 2019, **21**, 9590–9596.
- 53 P. Pykkö, *J. Phys. Chem. A*, 2015, **119**, 2326–2337.
- 54 T.-T. Chen, W.-L. Li, H. Bai, W.-J. Chen, X.-R. Dong, J. Li and L.-S. Wang, *J. Phys. Chem. A*, 2019, **123**, 5317–5324.
- 55 J.-L. Bredas, *Mater. Horiz.*, 2014, **1**, 17–19.
- 56 M. Rahm, T. Zeng and R. Hoffmann, *J. Am. Chem. Soc.*, 2019, **141**, 342–351.

